Optimization of the speed-skating technique for the straights

Joris Ravenhorst

Delft University of Technology

TU Delft

Optimization of the speedskating technique for the straights

by

Joris Ravenhorst

Student Name	Student Number
Joris Ravenhorst	4491319

Supervisor 1: Eline van der Kruk
Supervisor 2: Arend L. Schwab
Institution: Delft University of Technology
Faculty: Mechanical, Maritime and Materials Engineering, Delft
Department: Biomechanical Engineering
Graduation date: March 8th, 2023

Cover Image made by Joris Ravenhorst

Optimization of the speedskating technique for the straights

J.A. Ravenhorst (4491319)

Abstract— **The Dutch speedskating federation expressed the need for a feedback system for elite long-track speedskaters that can aid them in finding the optimal technique for an individual athlete. To contribute to this goal, this research aims to develop an optimization workflow that can reproduce realistic steady state speedskating behaviour. This is done with use of the simple skater model (SSM) (Van Der Kruk, Veeger, van der Helm, & Schwab, 2017). The research consists of two phases. The first to verify if the optimization can produce realistic speedskating motion, the second optimizes the speedskating technique to minimize the duration of one stroke. The optimization is solved with IPOPT. Even though the first phase can reproduce realistic speedskating motion, the optimal technique found in the second phase was unrealistic in terms of both trajectory and applied forces. This is caused by an inconsistency in the heading of the skate. This research shows the capabilities and limitations of optimizing the speedskating technique with the SSM.**

I. Introduction

Long-track speedskating is a unique and technical sport. Elite speedskaters excel because of their their physical condition and mastery of the technique. Still it is interesting to see how greatly the techniques differ between individual athletes. It is assumed that differences in body built and strength influence their personal optimal motion pattern. This makes it hard for athletes and their coaches to determine the optimal technique for each individual. On top of that, this is complicated because of the interconnectivity of the different variables that influence the speedskating technique such as leg extension, steering angle, lean angle and push-off force.

To aid the guidance and development of individual speedskaters, the Dutch speedskating federation (KNSB) expressed their need for a real time feedback system. Van der Kruk et al. (2018) took up this challenge and provided the first steps toward such a feedback system by developing and validating a simple biomechanical speedskater model (SSM) for the straight part of the ice rink (Van Der Kruk et al., 2017). This model simulates the speedskating technique and could potentially be used to find the optimal speedskating technique for individual speedskaters.

Allinger and Van Den Bogert (1997) have done research on optimizing steady state speedskating behaviour with a model similar to the SSM. However, the applicability of their results is limited, because the model is driven by a predetermined function describing the leg extension. Next to that both the model and the results of the optimizations have not been verified by measured kinetic data.

The aim of this study was to develop an optimization workflow that can reproduce realistic steady state speedskating behaviour. This can be the foundation of further research to provide insights into possible different optimal motion strategies for different body builds and strength.

II. Method

In this section first the SSM (Van Der Kruk et al., 2017) is described. Secondly the optimization problem, consisting of two phases, is defined. Lastly the optimization algorithm and the used settings are discussed.

A. Simple Skater Model

The SSM (Van der Kruk et al., 2018) is shown in figure 1. This section will give a short overview of the model and the equations of motion. The model was verified by 3D kinematic data and force data. It was shown that the model reproduces measured movement and forces with little error when the corresponding measured leg extension is used as input. This is different from the verification of the optimization done in this study, where it is investigated whether the optimization, subject to boundary conditions and constraints, can find optimal input (leg extension) and outputs (motion pattern of the skater and forces) to the model that approximate measured data. The kinematic data was collected by 20 motion capture cameras on 50 meter of the straight part of the ice rink, tracking 23 passive markers on the skater. The force data was measured by two skates instrumented with three-dimensional piezoelectric force sensors (Van Der Kruk, Den Braver, Schwab, Van der Helm, & Veeger, 2016).

1) Model description: This section summarizes the working principles of the SSM, as designed by Van Der Kruk et al. (2017). The SSM represents a skater as two point masses. Mass B is positioned at the estimated centre of mass of the whole body (COM) and mass S is positioned at the COM of the foot of the active skate on the ice. This way the model neglects the influence of arm movement, the double stance phase at which both skates are on the ice and the repositioning phase of the inactive skate in the air. Both masses have three degrees of freedom. For mass B these are three translations in the global x-,y-, and z-directions, and for mass S these consist of two horizontal translations (x- and y-directions), because the skate is assumed to be on the ice, and a steer angle θ_s. This steer angle describes the direction of the blade on the ice. It is assumed that the skate can only glide in this direction, therefore a non-holonomic constraint is applied to prevent lateral slip. A constant mass distribution coefficient η distributes the body mass of the skater over the two point masses. In this research the coefficient was first chosen to be the same as in the research by Van Der Kruk et al. (2017): $\eta = 0$, meaning the complete body mass is located at mass B.

The inputs of the model are coordinates u_s, v_s, w_s, θ_s, which describe the position of the skate relative to the COM

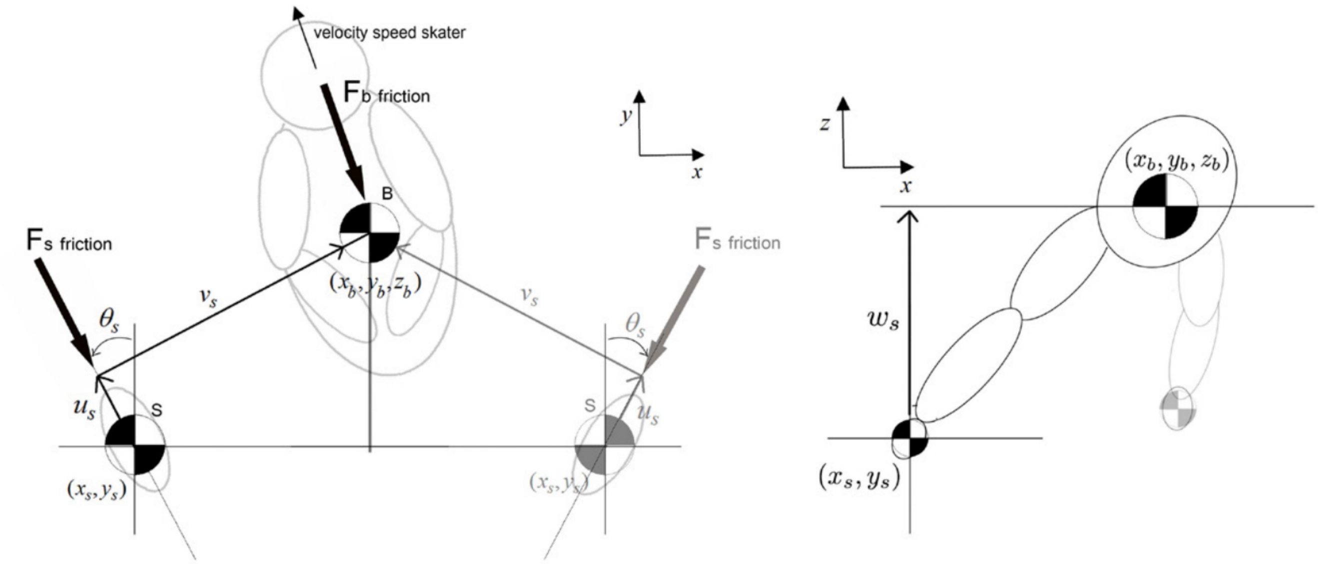

Fig. 1. Simple skater model as developed by Van Der Kruk et al. (2017). Left side: top view of the skater, right side: rear view of skater. Two point masses describe the skater: mass B (estimated at the COM of the full body) and mass S (positioned at the COM of the foot segment) describing the active skate on the ice.

and the steering angle. The distance between masses B and S will be indicated as the leg extension LL and is calculated as follows:

$$LL = \sqrt{u_{s,t}^2 + v_{s,t}^2 + w_{s,t}^2} \tag{1}$$

The outputs of the model are the global trajectory of mass B and the forces exerted by the skates on the ice.

2) Equations of motion: The equations of motions are formulated using the TMT method and are described in this sections.

Vector $\boldsymbol{x}$ contains the coordinates describing the global position and orientation of upper body B and skate S.

$$\boldsymbol{x} = \begin{bmatrix} x_b & y_b & z_b & x_s & y_s & \phi_s \end{bmatrix} \tag{2}$$

Instead of using this global representation, a minimum set of generalized coordinates $\boldsymbol{q}$ is used. This way the coordination of the skater can be expressed in terms of the leg extension and steering angle.

$$\boldsymbol{q} = \begin{bmatrix} u_b & v_b & w_s & u_s & v_s & \theta_s \end{bmatrix} \tag{3}$$

In eq. 3 coordinates (w_s, u_s, v_s) describe the leg extension and θ_s is the steering angle of the skate. (u_b, v_b) represent the generalized coordinates of the upper body and stand for the position in the global horizontal plane and will be a result of the system dynamics. With equations 2 and 3 and figure 1, a function T can be formulated which expresses the global coordinates in terms of the generalized coordinates.

$$\boldsymbol{x} = T(\boldsymbol{q}) \tag{4}$$

Which expanded becomes:

$$\begin{bmatrix} x_b \\ y_b \\ z_b \\ x_s \\ y_s \\ \phi_s \end{bmatrix} = \begin{bmatrix} u_b \\ v_b \\ w_s \\ u_b - kk \cdot \cos(\theta_s) \cdot v_s + kk \cdot \sin(\theta_s) \cdot u_s \\ v_b - \sin(\theta_s) \cdot v_s - \cos(\theta_s) \cdot u_s \\ kk \cdot \theta_s \end{bmatrix} \tag{5}$$

Here kk is a parameter describing which skate is active on the ice. (left skate: $kk = 1$, right skate: $kk = -1$). Derivation of T yields Jacobian matrix $\boldsymbol{T}$.

$$\dot{\boldsymbol{x}} = \frac{\partial T}{\partial \boldsymbol{q}} \dot{\boldsymbol{q}} = \boldsymbol{T}\dot{\boldsymbol{q}} \tag{6}$$

Jacobian matrix $\boldsymbol{T}$ maps global velocities onto generalized velocities and can also be used to transform global mass and force matrices into generalized mass and force matrices. Therefore, using the TMT method, the generalized mass matrix can be described as

$$\overline{\boldsymbol{M}} = \boldsymbol{T}^{\boldsymbol{T}} \boldsymbol{M} \boldsymbol{T} \tag{7}$$

with mass matrix $\boldsymbol{M}$

$$\boldsymbol{M} = \begin{bmatrix} m_b & 0 & 0 & 0 & 0 & 0 \\ 0 & m_b & 0 & 0 & 0 & 0 \\ 0 & 0 & m_b & 0 & 0 & 0 \\ 0 & 0 & 0 & m_s & 0 & 0 \\ 0 & 0 & 0 & 0 & m_s & 0 \\ 0 & 0 & 0 & 0 & 0 & I_s \end{bmatrix} \tag{8}$$

where m_b is the mass of B, m_s the mass of S and I_s the mass moment of inertia of S. Now the unconstrained equations of motion can be described in terms of generalized coordinates using Newton's law.

$$\overline{\boldsymbol{M}} \cdot \ddot{\boldsymbol{q}} = \overline{\boldsymbol{F}} \tag{9}$$

where $\ddot{\boldsymbol{q}}$ is the second time derivative of $\boldsymbol{q}$ and $\overline{\boldsymbol{F}}$ the reduced force matrix, which is defined as

$$\overline{\boldsymbol{F}} = \boldsymbol{T}^{\boldsymbol{T}} \left(\boldsymbol{f} - \boldsymbol{M} \cdot \boldsymbol{h}_{\text{con}} \right) + \boldsymbol{Q} \tag{10}$$

where $\boldsymbol{f}$ are external forces such as gravitational and friction forces, $\boldsymbol{h_{con}}$ are the convective acceleration terms of global coordinates $\boldsymbol{x}$ and $\boldsymbol{Q}$ are forces exerted on the local frame. The convective acceleration terms $\boldsymbol{h_{con}}$ are formulated as

$$\boldsymbol{h}_{con} = \frac{\partial \boldsymbol{T}}{\partial \boldsymbol{q} \cdot \partial \boldsymbol{q}} \dot{\boldsymbol{q}} \cdot \dot{\boldsymbol{q}} \tag{11}$$

Lastly, to complete the unconstrained equations of motion, the external forces are described as

$$\boldsymbol{f} = \begin{bmatrix} \sin(\theta_b) \cdot F_{b,f} \\ -\cos(\theta_b) \cdot F_{b,f} \\ -m_b \cdot g \\ kk \cdot \sin(\theta_s) \cdot F_{s,f} \\ -cos(\theta_s) \cdot F_{s,f} \\ kk \cdot M_s \end{bmatrix} \tag{12}$$

where g is the gravitational acceleration, M_s is the torque used to steer the skate, thus exerted on the skate in the horizontal plane. The two friction forces, ice friction (de Koning, De Groot, & van Ingen Schenau, 1992) and air friction (van Ingen Schenau, 1982), are described respectively as follows

$$F_{s,f} = \mu F_N \tag{13}$$

$$F_{b,f} = k_1 \boldsymbol{v}_{air}^2 \tag{14}$$

with ice friction coefficient μ, the normal force of the skate on the ice F_N (which is approximated by $F_N \approx m_{skater} g$), the velocity of the air relative to the skater$\boldsymbol{v}_{air}$ and k_1 a constant defined as

$$k_1 = \frac{1}{2} A C_d \rho \tag{15}$$

with drag coefficient C_d, frontal projected area of the skater A and air density ρ.

To finish the equations of motion, a non-holonomic constraint is formulated to prevent lateral movement of the skate.

$$C_s = -\sin(\theta_s)\dot{y}_s - kk\cos(\theta_s)\dot{x}_s = 0 \tag{16}$$

Expressing C_s in generalized coordinates and differentiating ones, yields the equation

$$\boldsymbol{C}\ddot{\boldsymbol{q}} + \boldsymbol{C}_{con} = 0 \tag{17}$$

where $\boldsymbol{C}$ is the Jacobian of the constraints and $\boldsymbol{C}_{con}$ are the convective acceleration terms of the constraints. This equation together with eq. 9 gives the complete set of equations of motion expressed in generalized coordinates:

$$\begin{bmatrix} \overline{\boldsymbol{M}} & \boldsymbol{C}^T \\ \boldsymbol{C} & \boldsymbol{0} \end{bmatrix} \begin{bmatrix} \ddot{\boldsymbol{q}} \\ \lambda \end{bmatrix} = \begin{bmatrix} \overline{\boldsymbol{F}} \\ -C_{con} \end{bmatrix} \tag{18}$$

with λ the Lagrange multiplier representing the constraint force acting lateral on the skate. $\overline{\boldsymbol{F}}$ is the reduced force matrix. The equations of motion (eq. 18) can be reorganized in terms of known ($\boldsymbol{q^o}$) and unknown ($\boldsymbol{q^d}$) coordinates.

$$\begin{bmatrix} \overline{\mathbf{M}}^{\mathbf{dd}} & \overline{\mathbf{M}}^{\mathbf{do}} & C^{d^T} \\ \overline{\mathbf{M}}^{\mathbf{od}} & \overline{\mathbf{M}}^{\mathbf{oo}} & C^{o^T} \\ C^d & C^o & 0 \end{bmatrix} \begin{bmatrix} \ddot{\boldsymbol{q}}^d \\ \ddot{\boldsymbol{q}}^o \\ \lambda \end{bmatrix} = \begin{bmatrix} \overline{\mathbf{F}}^{\mathbf{d}} \\ \overline{\mathbf{F}}^o \\ -C_{\text{con}} \end{bmatrix} \tag{19}$$

Here $\overline{\mathbf{F}}^o$ are the forces on the skate as a result of the leg extension:

$$\overline{\mathbf{F}}^{\mathbf{o}} = \begin{bmatrix} F_{w_s} & F_{u_s} & F_{v_s} & M_{\theta_s} \end{bmatrix} \tag{20}$$

Finally, when the weight of the COM is added to F_{w_s} we get the complete set of forces that the simulated skater exerts on the skate during the push-off.

$$\boldsymbol{F}_{push-off} = \begin{bmatrix} F_{w_s} + m_b g \\ F_{u_s} \\ F_{v_s} \end{bmatrix} \tag{21}$$

B. Problem description

This optimization research consisted of two phases. The first was designed to verify whether the optimization was able to reproduce realistic speedskating behaviour. The second was designed to find the optimal steady state speedskating technique to go as fast as possible. The general case that is optimized is one push-off stroke with the left skate where the COM travels a fixed forward distance. Apart from the objective functions and initial conditions, the constraints and state and input boundaries were the same for the two optimization phases. They will be discussed in the next sections. A summary is given in table IV in appendix II.

For the initial guess, simulated trajectories were used that were retrieved from the research by Van der Kruk et al. (2018). The initial guess functions as a starting point for the optimization. Simulated trajectories were used instead of measured data because differences between the optimal solution and the initial guess were then the result of the optimization and not partially because the model is unable to exactly reproduce measured trajectories. Different initial guesses were used in both optimization phases to evaluate the sensitivity of the optimization to the initial guess.

1) The general problem: As mentioned, the general problem is one push-off stroke with the left skate. The COM is tasked to travel a fixed forward distance while minimizing a cost function. The state of the system is described by the global position and velocity of the COM and the local position and velocity of the skate:

$$\boldsymbol{x} = \begin{bmatrix} x_b & y_b & \dot{x}_b & \dot{y}_b & u_s & v_s & w_s & \theta_s & \dot{u}_s & \dot{v}_s & \dot{w}_s & \dot{\theta}_s \end{bmatrix} \tag{22}$$

The input to the optimization is the acceleration of the skate relative to the COM:

$$\boldsymbol{u} = \left[\begin{array}{cccc} \ddot{u}_s & \ddot{v}_s & \ddot{w}_s & \ddot{\theta}_s \end{array}\right] \tag{23}$$

For comparison purposes, the forward distance traveled by the COM was chosen to equal the simulated covered distance of one stroke:

$$y_{b,t_f} = \tilde{y}_{b,t_f} \tag{24}$$

To make sure that the stroke with the left skate is repeatable also with the right skate and over the whole straight part of the ice rink, the following boundary conditions were set up: the velocity of the COM at the beginning and end of the stroke have to be equal in magnitude and direction, when mirroring the lateral component:

$$\begin{aligned} \dot{y}_{b,t_f} &= \dot{y}_{b,t_0} \\ \dot{x}_{b,t_f} &= -\dot{x}_{b,t_0} \\ \dot{w}_{b,t_f} &= \dot{w}_{b,t_0} \end{aligned} \tag{25}$$

Also the height of the COM should be the same at the beginning and end of the stroke:

$$w_{b,t_f} = w_{b,t_0} \tag{26}$$

Furthermore the distance between the COM and the skate is limited. With the leg fully extended this distance is approximated with the skater's leg length (LL) and in the crouched speedskating position this is approximated as half the leg length. Therefore the constraint on leg length becomes:

$$\frac{1}{2}LL \leq \sqrt{u_{s,t}^2 + v_{s,t}^2 + w_{s,t}^2} \leq LL \tag{27}$$

A second constraint is applied to prevent the skater from pulling laterally on the ice. This constraint appeared to be necessary during experimental optimizations. It means that when the left skate is laterally on the left side of the COM ($v_s > 0$), the lateral force component of the ice on the skate should be directed to the right ($F_v > 0$) and the other way around, with the skate on the right side of the COM ($v_s < 0$), the lateral force component of the ice on the skate should be directed to the left ($F_v < 0$). Therefore their product should be positive at all times:

$$v_{s,t} \cdot F_{v_s,t} \geq 0 \tag{28}$$

The third constraint limits the maximal push-off force that can be applied to the skate. The upper bound is based on the simulated data

$$0 \leq ||\boldsymbol{F}_{push-off}|| \leq 1300N \tag{29}$$

The lower and upper boundaries on states and inputs are quantified by looking at minimum and maximal values from simulations rounded upward in magnitude.

2) Phase 1, verification: To verify the ability to produce realistic speedskating behaviour, the results of this optimization were compared with simulated trajectories and force data. The objective was to find a duration of the stroke (t_f) as close as possible to the simulated duration of the stroke ($\tilde{t}_f$). So the objective function to be minimized becomes:

$$J_{PHASE1} = |\tilde{t}_f - t_f| \tag{30}$$

Next to that, the initial conditions were equal to the first time step of the simulated trajectory. Meaning the global position of the skate and COM and the velocities on that instant correspond to the simulation.

This optimization was done four times with different initial guesses. The guesses are based on two simulations by the SSM based on different skaters, denoted by A and B:
- guess A1: The complete trajectory of simulation A.
- guess A2: The initial and final time steps of simulation A.
- guess A3: The initial and final time steps of a manually designed straight line trajectory with zero inputs.
- guess B1: The complete trajectory of simulation B.

Constants for leg length, body mass, air friction, and the covered forward distance differ between simulations A and B. The values are given in table I and are adopted in the optimization, meaning that apart from the initial guess, also these parameters differ between optimizations based on simulations A and B. This has to be taken into account when comparing the optimal results.

TABLE I
CONSTANTS USED FOR OPTIMIZATIONS WITH INITIAL GUESSES BASED ON SIMULATION A AND B.

Parameter	Description	Value
g	gravitational acceleration	9.81 m/s^2
α	mass distribution coefficient	0
μ	ice friction coefficient	0.006
k_1	air friction constant (A, B)	0.18, 0.14 m^2/s^2
m	skater's body mass (A, B)	65, 76 kg
LL	leg length (A, B)	1.1, 1.2 m
$\lvert y_{b,f} - y_{b,0}\rvert$	fixed forward distance (A, B)	9.36, 14.5 m
$\tilde{t}_f$	duration of the simulated stroke (A, B)	0.98, 1.29 s

The results of optimizing phase 1 consist of the minimized cost and figures describing the optimal solutions compared to the simulation. By means of these results it is analysed whether the optimization is able to reproduce realistic speedskating behaviour. Also the sensitivity of the optimization to the initial guess is investigated.

3) Phase 2, performance: Phase 2 was designed to optimize speed skating performance. The objective is to minimize the duration of the stroke t_f.

$$J_{PHASE2} = t_f \tag{31}$$

Contrary to phase 1, the initial state conditions ($t = 0$) are free to be determined by the optimization algorithm subject to the bounds and constraints presented in table IV in appendix II. Only the initial position of the COM in the horizontal plane is predetermined to be the same as the

TABLE II

OPTIMIZATION SETTINGS, AS REQUESTED IN ICLOCS2

Primary settings		**Sub settings**	
transcription method:	direct collocation	amount of nodes	50
		error criteria	local absolute error
		discretization	Hermite-Simpson method
		derivative generation	numeric
NLP solver:	IPOPT	convergence tolerance	1e-3
		max iterations	500
		barrier parameter update strategy	monotone
		Hessian approximation	exact
meshing strategy:	no mesh refinements		

measurement for comparison purposes. The initial velocity of the COM is free to be determined by the optimization.

Additionally to the constraints and boundary conditions of phase 1, one general constraint and one constraint on the initial conditions are added to the optimization. First, the constraint on the initial conditions is to make sure the skater begins in the characteristic crouched pose. Therefore the leg extension is bounded. The bounds are based on observed data from Van Der Kruk et al. (2017):

$$0.65 \cdot LL \leq \sqrt{u_{s,t_0}^2 + v_{s,t_0}^2 + w_{s,t_0}^2} \leq 0.75 \cdot LL \qquad (32)$$

The second constraint is formulated to restrict leg extension velocity. Which is calculated as the first time derivative of the leg extension. The bounds are based on the simulated values:

$$-0.1 \leq \dot{LL} \leq 0.6 \qquad (33)$$

For the optimization of phase 2 initial guesses $A.1$ and $B.1$ are used because they yield good reproduction of the simulated speedskating technique in phase 1.

The results of optimizing phase 2 consist of the minimized cost and figures of the trajectory and push-off force. For further investigation of the feasibility of the results additional figures will are provided of the leg extension and the directions of applied forces. By means of these results it is analysed whether the optimal solution is successful. This is the case when the duration of the stroke is minimized to a relevant amount and the optimal technique is plausible.

C. Optimization algorithm

The optimization was done using the ICLOCS2 toolbox in Matlab (Nie, Faqir, & Kerrigan, 2018). The toolbox provides guidance for formulating optimal control problems and includes a variety of transcription methods and non-linear problem (NLP) solvers.

In general, an optimal control problem seeks to minimize or maximize a certain performance index which depends on the state and control of a dynamic system, subject to constraints and boundary conditions. This results in a set of non-linear differential equations and integrating functions. These are often solved in two steps. The first being solving the differential equations and integrating functions using a transcription method and the second solving the NLP with an appropriate solver. (Rao, 2009).

In this research direct collocation was used as transcription method and IPOPT as an NLP solver. Direct collocation has been widely used in similar biomechanical optimization research (Ackermann and Van den Bogert (2010), Kaplan and Heegaard (2001), Brown and McPhee (2020)) and has been proven to perform better than other conventional algorithms such as shooting methods in terms of computation time (Porsa, Lin, and Pandy (2016), Lee and Umberger (2016)). Also, the direct collocation method is well suited for problems with constraints that apply at the end of the simulation, such as constraints for periodicity (Van Den Bogert, Blana, & Heinrich, 2011) as will be used in this research. Direct collocation discretizes the continuous optimization problem. By approximating the continuous trajectory by multiple polynomials. This means that the problem is divided into pieces represented by a small (finite) set of coefficients and it becomes easier to calculate integrals and derivatives (Kelly, 2017).

IPOPT is an open source interior point NLP solver developed by the COIN-OR Foundation (Wächter & Biegler, 2006) and has been used successfully in combination with direct collocation in previous biomechanical optimization studies (Laschowski, Mehrabi, and McPhee (2018), Van den Bogert, Hupperets, Schlarb, and Krabbe (2012), Nitschke et al. (2020)). Also, computation time with IPOPT can be similar or smaller compared to fmincon, an NLP solver included in Matlab (Lee & Umberger, 2016). As mentioned, IPOPT makes use of an interior point algorithm. In short, the interior point method is a gradient method that approximates inequality constraints by barrier functions (Wächter & Biegler, 2006).

1) Solver settings: ICLOCS provides an insightful way to configure the optimization algorithm. The main settings are presented in table II. These settings were chosen because they provided the shortest computation time or were recommended by the developers for this application (Nie et al., 2018). Additionally the error tolerances of all boundary and constraint violations are set to 0.01.

III. RESULTS

In this section the results of both phases are presented consecutively.

A. Phase 1

In phase 1 the objective was to minimize the difference between the duration of the optimized stroke and the durations

TABLE III

MINIMIZED COSTS FOR OPTIMIZATIONS BASED ON GUESSES A1, A2, A3 AND B1.

	A1	A2	A3	B1
cost $[s]$	0.0073	0.0096	0.0128	0.0058

of the simulated stroke (eq. 30). This was repeated with four different initial guesses. The minimized costs are presented in table III for each optimization. The lowest cost is achieved in the optimization based on B1. From the three guesses based on simulation A the guess with the full trajectory (A1) results in the lowest cost, followed by A2 and then A3. This order in performance emerges also when looking at the optimized trajectories (figure 2). With guesses A1 and B1 the trajectories of the skate and COM in the optimal solution stay very close to the simulation. The positioning of the skate relative to the COM is best with guess A1, as can be seen by the lines connecting the skate and COM at every 5th time step. The trajectories found from guess A2 are similar in shape to the simulation, only with larger lateral displacement. Also the positioning of the skate is more backward compared to the simulation. The trajectories found from guess A3 are not similar to the simulation, showing lateral displacement to the right instead of to the left.

Also the push-off force is best reproduced by optimizing from guess A1 compared to A2 and A3 (figure 3). The push-off force found from optimization B1 performs similar to optimization A1 (appendix I, figure 8).

Initial guesses A1 and B1 also yield faster and more steady convergence than A2 and A3. This can be seen in figure 10 in appendix I. With A1 and B1 it takes less function evaluations to find the optimal solution. The convergence of optimization A2 shows large fluctuations in evaluated costs.

B. Phase 2

Phase 2 minimizes the duration of one stroke. This optimization was repeated with two initial guesses of complete simulated trajectories of the skate and COM A1 and B1. With guess A1 the duration of the stroke was minimized to $0.1378s$ and with B1 to $0.2193s$, leading to average forward velocities of respectively $67.9m/s$ and $66.1m/s$. For comparison, the duration of the corresponding simulations are $0.98s$ and $1.29s$ respectively. The trajectories of both solutions are shown in figure 4. Here it can be seen that both initial guesses lead to the same movement strategy: straight forward trajectories of the skate and the COM. The lateral distance of the skate relative to the COM is smaller in the optimal solution from B1 compared to the optimal solution from A1, but this is also the case when comparing the simulated trajectories of guesses A1 and B1. Overall the optimal trajectories do not resemble the simulated trajectories.

In both optimal solutions A1 and B1 the maximal allowed push-off force is exerted for the complete duration of the stroke. The push-off force from solution A1 is shown in figure 5 and from solution B1 in appendix I figure 9.

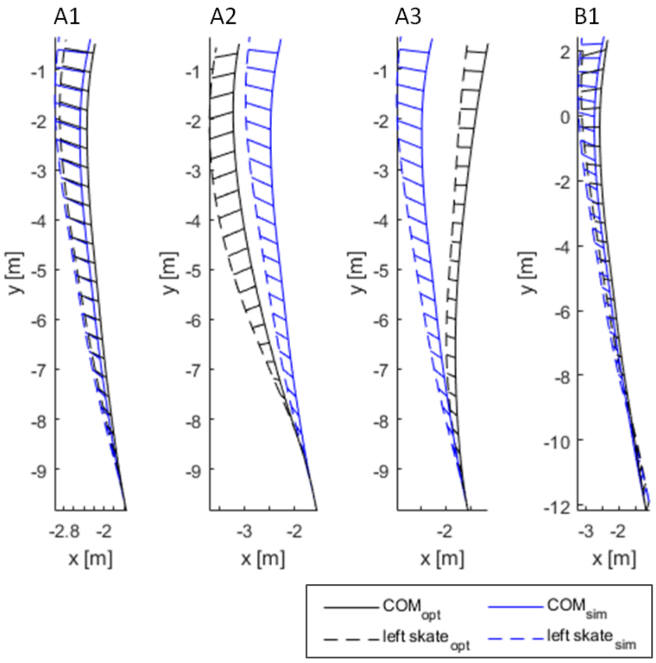

Fig. 2. Phase 1. Top views of the optimal and simulated trajectories of the left skate (dashed line) and the COM (continuous line). Separately for initial guesses A1, A2, A3 and B1. The lines connecting the COM and the skate represent the leg extension. x is the lateral and y the forward direction.

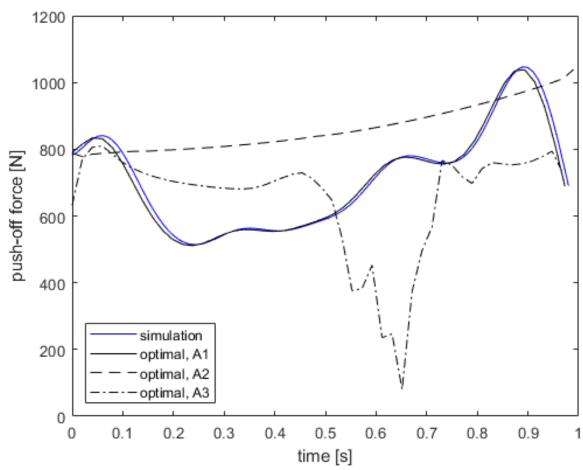

Fig. 3. Phase 1. Push-off force of the optimal solutions and the simulation. Separately for initial guesses A1, A2 and A3.

The convergence of both solutions are presented in appendix I, figure 11. In both cases the convergence is good.

For further investigation of the optimal solutions of phase 2 a closer look is taken of the forces acting on the skate and the COM. In figure 6 the forces acting on the skate and COM are shown at one time instant in optimal solution A1. Because of the straight line trajectories the direction and proportion of the forces is similar at each time step. Here the ice friction F_s is very small relative to the other forces and therefore hard to see. The vector is perpendicular to λ and $F_{push-off}$ and points in the direction of positive x and negative y.

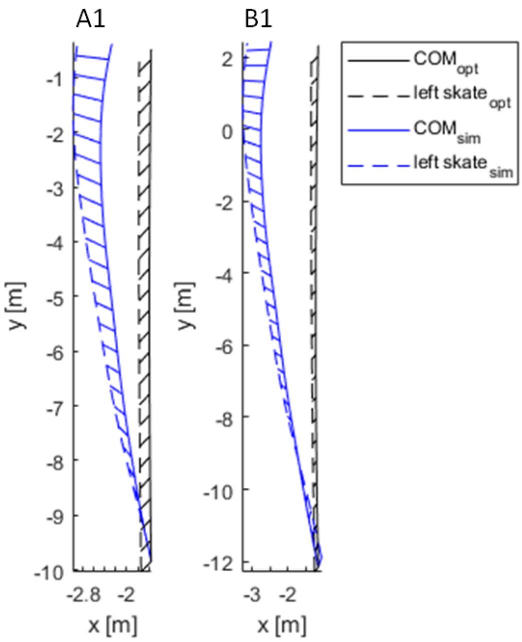

Fig. 4. Phase 2. Top views of the optimal and simulated trajectories of the left skate (dashed line) and the COM (continuous line). Separately for initial guesses A1 and B1. The lines connecting the COM and the skate represent the leg extension. x is the lateral and y the forward direction.

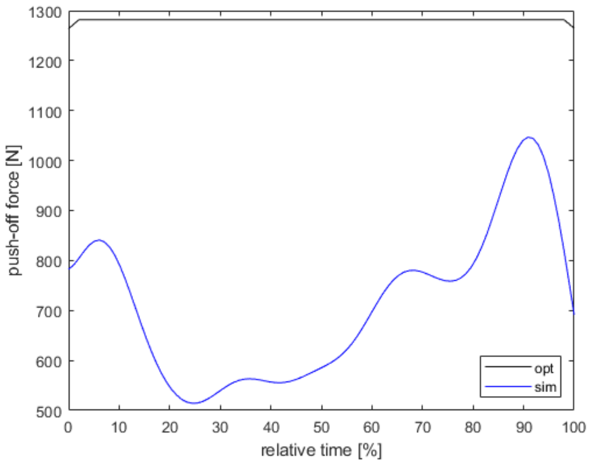

Fig. 5. Phase 2. Push-off force from optimal solution A1 and the simulation..

Here it can be seen that λ is not perpendicular to the trajectory of the skate, which it should be due to the non-holonomic constraint restricting lateral slipping of the skate (16). Numerical evaluation of this constraint indeed shows that the outcome is not zero for all time steps. The deviation between the heading of the skate θ_s and the trajectory of the skate ranges between 34.9 and 35.5 degrees. For the optimization from guess B1 this ranges between 34.8 and 35.7 degrees. Because of this error, the non-holonomic constraint has also been evaluated for phase 1 and for the simulations. In phase 1 the deviation ranges were $[1.53\ 2.17]$ and $[1.56\ 2.00]$ degrees for A1 and B1 respectively. For simulations A and B the deviations were $[-0.834\ 1.64]$ and $[-0.607\ 1.70]$ degrees respectively.

Air friction F_b is opposite to the trajectory of the COM and is in the y-direction almost equal in magnitude to the y-component of $F_{push-off}$ acting on the COM.

Lastly the leg extension is investigated. Figure 7 shows the leg extension and leg extension velocity of the optimal solution with initial guess A1. Here it can be seen that the optimal solution starts with a larger leg extension compared to the simulation. Also the optimal leg extension velocity and the simulated leg extension velocity have roughly the same steepness in the duration of the optimal stroke. Interestingly the optimal leg extension velocity begins negative, meaning the leg extension decreases before increasing. In the leg extension plot in figure 7 it can be seen that this decrease in leg length is very small. For optimization from initial guess B1 the leg extension looks similar (appendix I, figure 12).

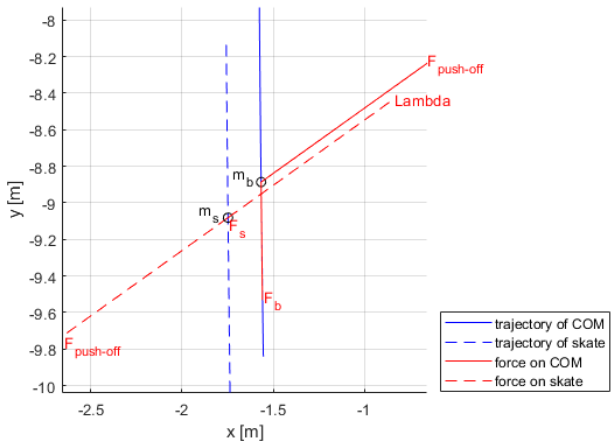

Fig. 6. Phase 2. Top view of the forces acting on the skate and the COM, projected on the horizontal plane. Positive y is the forward direction. The force vectors are scaled. Ice friction F_s is very small relative to the other forces and therefore hard to see. The vector is perpendicular to λ and points in the direction of negative x and negative. m_s and m_b are the point masses of the skate and COM respectively.

IV. Discussion

The aim of this study was to develop an optimization workflow that can reproduce one realistic steady state speed-skating stroke when minimizing the duration. Optimization phase 1, minimizing the difference between the optimized and simulated duration of the stroke, produces realistic speedskating motion. Optimization phase 2, minimizing the duration of the optimized stroke, was however unable to find a solution resembling realistic speedskating motion. The next two sections discuss the outcomes of intermediate optimization phase 1 and the final outcomes of the study in phase 2.

A. *Influence initial guess*

In phase 1 the importance of a good initial guess becomes apparent. When a complete trajectory of a simulated speed-skating stroke is used as initial guess the optimal solution

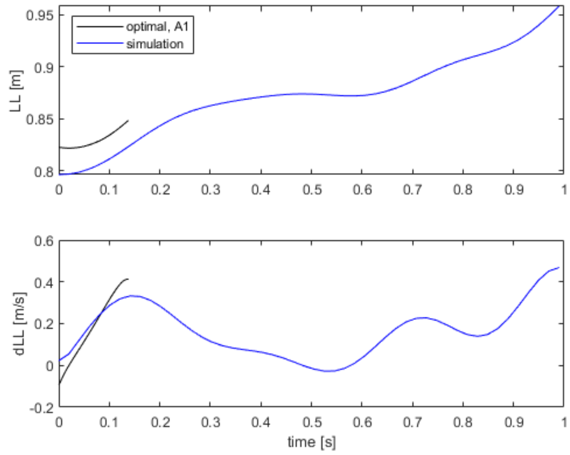

Fig. 7. Phase 2. Leg extension characteristics of the optimal solution from initial guess A1, compared to the simulation. With the top figure showing the effective leg extension (distance between the skate and the COM). The bottom figure shows the leg extension velocity

resembles simulated trajectories and push-off force. Also the convergence is fast and smooth. The increase of the cost during the first function evaluations appears because the trajectory that is used as initial guess does not satisfy the boundary constraints of cyclic motion. Therefore the guess and the first optimization iterations close to the guess are infeasible solutions, urging the optimization to find a different solution.

Also it is clear that when a complete trajectory is used as initial guess the optimal solution stays close to the guess. This is especially apparent in phase 1 (fig. 2), but is also seen in phase 2, where the main difference between the solutions of A1 and B1 is the same as between the simulated trajectories A and B: A1 shows a larger lateral distance between the skate and the COM (fig. 4). However, this could also be caused by the difference in certain constants used in the optimization (table I). Therefore more research should be done to evaluate the sensitivity of the optimization to the initial guess and the constant parameters.

B. Feasibility of results

Even though optimization phase 1 is able to reproduce realistic speedskating motion given a complete simulated trajectory as initial guess, this is not the case for phase 2. In phase 2 the optimal trajectories and push-off force do not resemble the simulations and the optimized average forward velocities (67.9 and $66.1 m/s$) are unrealistically high. It appears that the optimization can achieve these velocities because the non-holonomic constraint (eq. 16) is not satisfied. This way the model is able to follow a straight forward trajectory with the skate and still generating a push-off force in the forward direction. If the non-holonomic constraint would be satisfied, the constraint force λ should be perpendicular to the skate trajectory and therefore in this case of the forward straight trajectory directed in the lateral direction. This way also the push-off force should not be able to have such a large contribution to the forward motion and should this trajectory result in a much slower trajectory.

While the unsatisfied non-holonomic constraint causes the results of phase 2 to be infeasible, the results of phase 1 were satisfactory. Here it has also been noticed that there existed deviations between the steering angle of the skate and the direction of the skate's trajectory, but the range of the deviations were smaller than found for the simulations. Possibly these small errors found for phase 1 and the simulations are caused by the differentiation of the skate's position in order to evaluate the constraint. However, the large errors in phase 2 indicate that there exists a problem in the working of the non-holonomic constraint. This could be caused by the coupling of the heading of the skate and the direction of the skate's trajectory or the application of the non-holonomic constraint.

Apart from the direction of the push-off force and the trajectories being inconsistent with a realistic speedskating behaviour, also the relation of the push-off force to the leg extension is not realistic. As was seen in figure 7 in the results, the optimal leg extension and the simulated leg extension do not differ much in shape in the duration of the optimal stroke. The difference is mainly that the optimal leg extension velocity begins negative and the leg extension's initial value is larger. Still the model is able to exert the maximal allowed push-off force during the complete stroke (fig. 5). Biomechanically this is unrealistic. The force is related to the length and velocity of the leg extension. Existing research on these relations mostly focus on joint torque, angle and angular velocity of individual joints ((Hahn, Herzog, & Schwirtz, 2014), (Thorstensson, Grimby, & Karlsson, 1976), (Coyle, Costill, & Lesmes, 1979)). Such relations would require the addition of individual joints to the model, increasing the complexity. Also linear force-velocity and parabolic power-velocity relations have been found for leg extensions in ballistic push-offs: exercises like squats and leg-presses ((Morin & Samozino, 2018)). These relations could provide useful upper boundaries for the optimization, although the ballistic exercises mainly involve extension and flexion of the lower limb joints, while in the skating technique also abduction of the hip is involved. This influences the applicability of the found relationships. This is a subject for further research.

V. Conclusion

In this section the main conclusions of this speedskating optimization study are summarized. One speedskating push-off was optimized subject to two objectives consecutively. In phase 1 the objective was to minimize the difference between the duration of the optimal stroke and the duration of a simulated speedskating stroke. With the goal to verify whether the optimization is able to reproduce realistic speedskating behaviour. In phase 2 the duration of the optimized stroke was minimized.

When given complete simulated trajectories of the skate and COM as initial guess, the optimization of phase 1 reproduces the simulated speedskating technique closely in both trajectories and push-off force. This satisfactory result was obtained when using two different simulations as initial guess.

It was noticed that the initial guess influences the optimal solution. In phase 1, when using only the initial and final conditions of the simulation as initial guess or using the initial and final conditions of a straight line trajectory as initial guess, then the optimal solutions differ greatly from the simulations. As said, when using complete simulated trajectories as initial guess, the optimal solution stays very close to those simulations. This is also noticed in phase 2. Even though the optimal trajectories do not resemble the simulations, certain characteristic differences between the two simulations emerge also in the corresponding optimal solutions. This could however also be caused by the differences in used constant parameters such as the body mass and leg length of the modelled skater. Therefore further research is needed on the sensitivity of the optimization to the initial guess and the constant parameters that are used.

The results of phase 2 did not resemble realistic speedskating behaviour. The skate and COM follow straight forward trajectories and the maximal allowed peak push-off force is maintained for the complete duration of the stroke. This result was similar with both simulations as initial guess. Interestingly, this result should be infeasible for the model (Van Der Kruk et al., 2017) because the variable determined as the heading of the skate did not correspond to the direction of the trajectory of the skate. This should be prevented by a non-holonomic constraint inhibiting lateral slipping of the skate. It has to be investigated whether the coupling of the heading of the skate and the direction of the skate's trajectory is correct and whether the non-holonomic constraint is implemented properly.

References

Ackermann, M., & Van den Bogert, A. J. (2010). Optimality principles for model-based prediction of human gait. *Journal of biomechanics*, *43*(6), 1055–1060.

Allinger, T. L., & Van Den Bogert, A. J. (1997). Skating technique for the straights, based on the optimization of a simulation model. *Medicine and science in sports and exercise*, *29*(2), 279–286.

Brown, C., & McPhee, J. (2020). Predictive forward dynamic simulation of manual wheelchair propulsion on a rolling dynamometer. *Journal of biomechanical engineering*, *142*(7), 071008.

Coyle, E. F., Costill, D. L., & Lesmes, G. R. (1979). Leg extension power and muscle fiber composition. *Med Sci Sports*, *11*(1), 12–15.

de Koning, J. J., De Groot, G., & van Ingen Schenau, G. J. (1992). Ice friction during speed skating. *Journal of biomechanics*, *25*(6), 565–571.

Hahn, D., Herzog, W., & Schwirtz, A. (2014). Interdependence of torque, joint angle, angular velocity and muscle action during human multi-joint leg extension. *European journal of applied physiology*, *114*, 1691–1702.

Kaplan, M. L., & Heegaard, J. H. (2001). Predictive algorithms for neuromuscular control of human locomotion. *Journal of Biomechanics*, *34*(8), 1077–1083.

Kelly, M. (2017). An introduction to trajectory optimization: How to do your own direct collocation. *SIAM Review*, *59*(4), 849–904.

Laschowski, B., Mehrabi, N., & McPhee, J. (2018). Optimization-based motor control of a paralympic wheelchair athlete. *Sports Engineering*, *21*(3), 207–215.

Lee, L.-F., & Umberger, B. R. (2016). Generating optimal control simulations of musculoskeletal movement using opensim and matlab. *PeerJ*, *4*, e1638.

Morin, J.-B., & Samozino, P. (2018). Biomechanics of training and testing. *Biomechanics of Training and Testing: Innovative Concepts and Simple Field Methods. New York, NY: Springer International Publishing. https://doi. org/10.1007/978-3-319-05633-3*.

Nie, Y., Faqir, O., & Kerrigan, E. C. (2018). Iclocs2: Solve your optimal control problems with less pain.

Nitschke, M., Dorschky, E., Heinrich, D., Schlarb, H., Eskofier, B. M., Koelewijn, A. D., & van den Bogert, A. J. (2020). Efficient trajectory optimization for curved running using a 3d musculoskeletal model with implicit dynamics. *Scientific reports*, *10*(1), 1–12.

Porsa, S., Lin, Y.-C., & Pandy, M. G. (2016). Direct methods for predicting movement biomechanics based upon optimal control theory with implementation in opensim. *Annals of biomedical engineering*, *44*(8), 2542–2557.

Rao, A. V. (2009). A survey of numerical methods for optimal control. *Advances in the Astronautical Sciences*, *135*(1), 497–528.

Thorstensson, A., Grimby, G., & Karlsson, J. (1976). Force-velocity relations and fiber composition in human knee extensor muscles. *Journal of applied physiology*, *40*(1), 12–16.

Van Den Bogert, A. J., Blana, D., & Heinrich, D. (2011). Implicit methods for efficient musculoskeletal simulation and optimal control. *Procedia Iutam*, *2*, 297–316.

Van den Bogert, A. J., Hupperets, M., Schlarb, H., & Krabbe, B. (2012). Predictive musculoskeletal simulation using optimal control: effects of added limb mass on energy cost and kinematics of walking and running. *Proceedings of the Institution of Mechanical Engineers, Part P: Journal of Sports Engineering and Technology*, *226*(2), 123–133.

Van Der Kruk, E., Den Braver, O., Schwab, A. L., Van der Helm, F. C., & Veeger, H. (2016). Wireless instrumented klapskates for long-track speed skating. *Sports Engineering*, *19*(4), 273–281.

Van Der Kruk, E., Veeger, H., van der Helm, F., & Schwab, A. (2017). Design and verification of a simple 3d dynamic model of speed skating which mimics observed forces and motions. *Journal of biomechanics*, *64*, 93–102.

Van der Kruk et al., E. (2018). *Parameter analysis for speed skating performance* (Unpublished doctoral dissertation). Delft University of Technology.

van Ingen Schenau, G. J. (1982). The influence of air friction in speed skating. *Journal of Biomechanics*, *15*(6), 449–458.

Wächter, A., & Biegler, L. T. (2006). On the implementation of an interior-point filter line-search algorithm for large-scale nonlinear programming. *Mathematical programming*, *106*(1), 25–57.

APPENDIX I
ADDITIONAL FIGURES

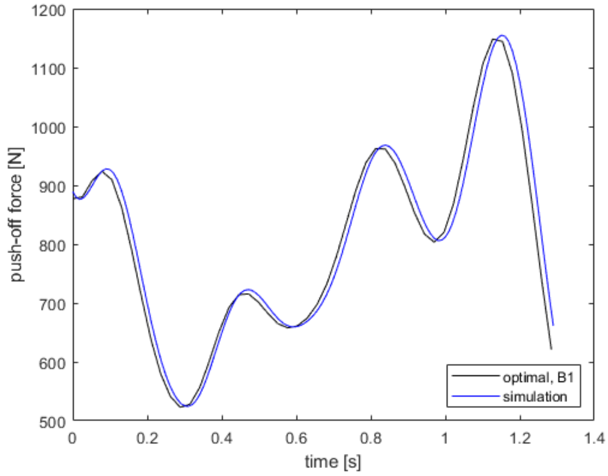

Fig. 8. Phase 1. Push-off force of the optimal solution from initial guess B1 and the simulation.

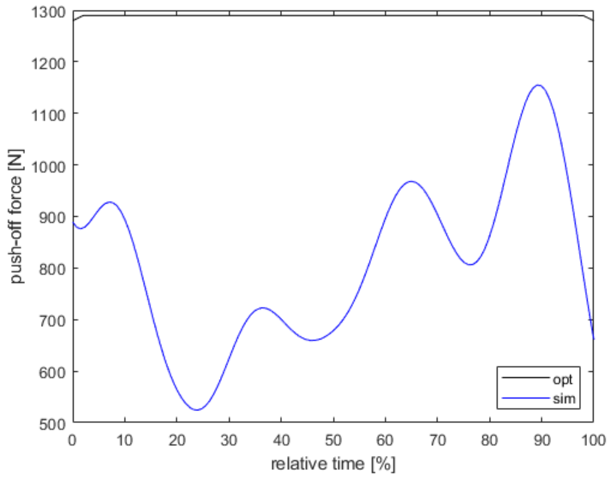

Fig. 9. Phase 2. Push-off force of the optimal solution from initial guess B1 and the simulation.

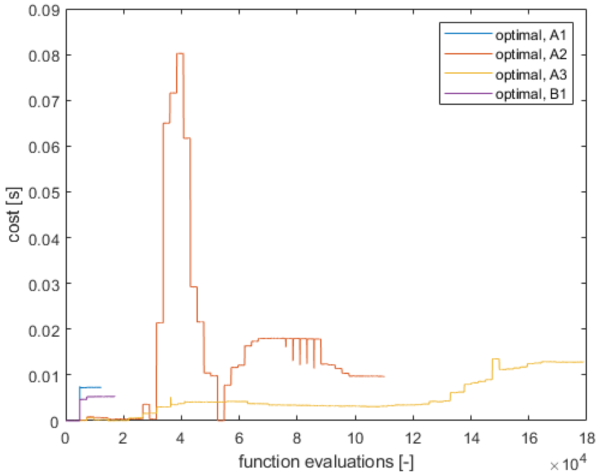

Fig. 10. Phase 1. Convergence of optimizations based on initial guesses A1, A2, A3 and B1.

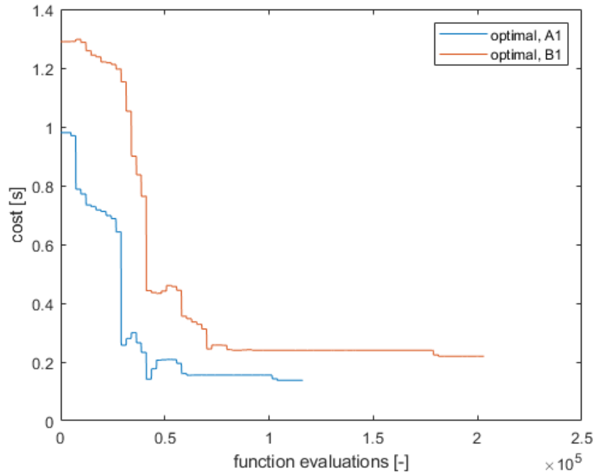

Fig. 11. Phase 2. Convergence of optimizations from initial guess A1 and B1.

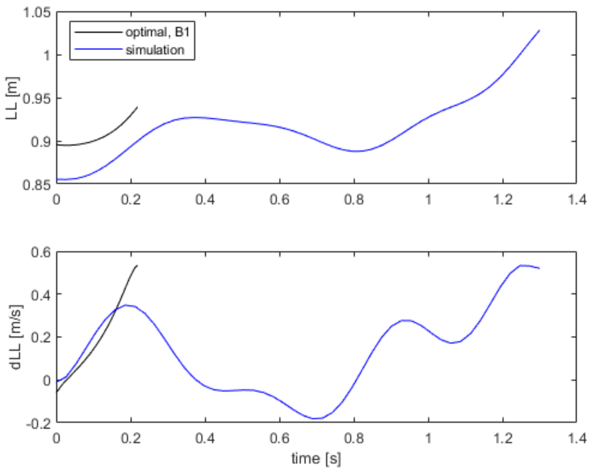

Fig. 12. Phase 2. Leg extension characteristics of the optimal solution from initial guess B1, compared to the simulation. With the top figure showing the effective leg extension (distance between the skate and the COM). The bottom figure shows the leg extension velocity.

Appendix II
Problem definition table, displayed on next page

TABLE IV

PROBLEM DEFINITION OF THE TWO OPTIMIZATION PHASES. WITH INPUTS $\boldsymbol{u} = \begin{bmatrix}\ddot{u}_s & \ddot{v}_s & \ddot{w}_s & \ddot{\theta}_s\end{bmatrix}$ AND STATES $\boldsymbol{x} = \begin{bmatrix} x_b & y_b & \dot{x}_b & \dot{y}_b & u_s & v_s & w_s & \theta_s & \dot{u}_s & \dot{v}_s & \dot{v}_s & \dot{\theta}_s \end{bmatrix}$. $\tilde{x}$ REPRESENTS THE SIMULATED EQUIVALENT OF VARIABLE x.

		PHASE1	PHASE2
Cost function		$J^{PHASE1} = \lvert t_f - \tilde{t}_f \rvert$	$J^{PHASE2} = t_f$
Constraints	Fixed distance	$y_{b,t_f} = \tilde{y}_{b,t_f}$	$y_{b,t_f} = \tilde{y}_{b,t_f}$
	Cyclic motion	$\dot{y}_{b,t_f} = \dot{y}_{b,t_0}$ $\dot{x}_{b,t_f} = -\dot{x}_{b,t_0}$ $\dot{w}_{b,t_f} = \dot{w}_{b,t_0}$ $w_{b,t_f} = w_{b,t_0}$	$\dot{y}_{b,t_f} = \dot{y}_{b,t_0}$ $\dot{x}_{b,t_f} = -\dot{x}_{b,t_0}$ $\dot{w}_{b,t_f} = \dot{w}_{b,t_0}$ $w_{b,t_f} = w_{b,t_0}$
	Leg length	$1/2LL \leq \sqrt{u_{s,t}^2 + v_{s,t}^2 + w_{s,t}^2} \leq LL$	$1/2LL \leq \sqrt{u_{s,t}^2 + v_{s,t}^2 + w_{s,t}^2} \leq LL$
	No pulling forces	$v_{s,t} \cdot F_{v_{s,t}} \geq -8$	$v_{s,t} \cdot F_{v_{s,t}} \geq -8$
	Max force on skate	$0 \leq \lVert \boldsymbol{F}_{skate,t} \rVert \leq 1300$	$0 \leq \lVert \boldsymbol{F}_{skate,t} \rVert \leq 1300$ $-0.1 \leq \dot{LL} \leq 0.6$
Control boundaries		$\mathbf{u}^{lb} = \begin{bmatrix}-20 & -20 & -20 & -16\pi\end{bmatrix}$ $\mathbf{u}^{ub} = \begin{bmatrix}24 & 30 & 10 & 6\pi\end{bmatrix}$	$\mathbf{u}^{lb} = \begin{bmatrix}-20 & -20 & -20 & -16\pi\end{bmatrix}$ $\mathbf{u}^{ub} = \begin{bmatrix}24 & 30 & 10 & 6\pi\end{bmatrix}$
State boundaries		$\mathbf{x}^{lb} = [-5 \;\; \tilde{y}_{b,t_0} \;\; -5 \;\; 8 \;\; \ldots \;\; -0.4 \;\; -LL \;\; 0.5LL \;\; -0.2\pi \;\; \ldots \;\; -3.2 \;\; -3.2 \;\; -3.2 \;\; -0.5\pi]$ $\mathbf{x}^{ub} = [5 \;\; \tilde{y}_{b,t_f} \;\; 5 \;\; 25 \;\; \ldots \;\; 0.6 \;\; LL \;\; LL \;\; 0.2\pi \;\; \ldots \;\; 3.2 \;\; 3.2 \;\; 3.2 \;\; 0.5\pi]$	$\mathbf{x}^{lb} = [-5 \;\; \tilde{y}_{b,t_0} \;\; -5 \;\; 8 \;\; \ldots \;\; -0.4 \;\; -LL \;\; 0.5LL \;\; -0.2\pi \;\; \ldots \;\; -3.2 \;\; -3.2 \;\; -3.2 \;\; -0.5\pi]$ $\mathbf{x}^{ub} = [5 \;\; \tilde{y}_{b,t_f} \;\; 5 \;\; 25 \;\; \ldots \;\; 0.6 \;\; LL \;\; LL \;\; 0.2\pi \;\; \ldots \;\; 3.2 \;\; 3.2 \;\; 3.2 \;\; 0.5\pi]$
Initial conditions		$\mathbf{x}_{t_0} = \tilde{\mathbf{x}}_{t_0}$	$\mathbf{x}_{t_0}^{lb} = [\tilde{x}_{b,t_0} \;\; \tilde{y}_{b,t_0} \;\; -5 \;\; 8 \;\; \ldots \;\; -0.4 \;\; -LL \;\; 0.5LL \;\; -0.2\pi \;\; \ldots \;\; -3.2 \;\; -3.2 \;\; -3.2 \;\; -0.5\pi]$ $\mathbf{x}_{t_0}^{ub} = [\tilde{x}_{b,t_0} \;\; \tilde{y}_{b,t_0} \;\; 5 \;\; 25 \;\; \ldots \;\; 0.6 \;\; LL \;\; LL \;\; 0.2\pi \;\; \ldots \;\; 3.2 \;\; 3.2 \;\; 3.2 \;\; 0.5\pi]$ $0.65 \cdot LL \leq \sqrt{u_{s,t_0}^2 + v_{s,t_0}^2 + w_{s,t_0}^2} \leq 0.75 \cdot LL$
Terminal state bounds		$\mathbf{x}_{t_f}^{lb} = [-5 \;\; \tilde{y}_{b,t_f} \;\; -5 \;\; 8 \;\; \ldots \;\; -0.4 \;\; -LL \;\; 0.5LL \;\; -0.2\pi \;\; \ldots \;\; -3.2 \;\; -3.2 \;\; -3.2 \;\; -0.5\pi]$ $\mathbf{x}_{t_f}^{ub} = [5 \;\; \tilde{y}_{b,t_f} \;\; 5 \;\; 25 \;\; \ldots \;\; 0.6 \;\; LL \;\; LL \;\; 0.2\pi \;\; \ldots \;\; 3.2 \;\; 3.2 \;\; 3.2 \;\; 0.5\pi]$	$\mathbf{x}_{t_f}^{lb} = [-5 \;\; \tilde{y}_{b,t_f} \;\; -5 \;\; 8 \;\; \ldots \;\; -0.4 \;\; -LL \;\; 0.5LL \;\; -0.2\pi \;\; \ldots \;\; -3.2 \;\; -3.2 \;\; -3.2 \;\; -0.5\pi]$ $\mathbf{x}_{t_f}^{ub} = [5 \;\; \tilde{y}_{b,t_f} \;\; 5 \;\; 25 \;\; \ldots \;\; 0.6 \;\; LL \;\; LL \;\; 0.2\pi \;\; \ldots \;\; 3.2 \;\; 3.2 \;\; 3.2 \;\; 0.5\pi]$